ACS MATERIALS LETTERS

www.acsmaterialsletters.org

LETTER

Mechanochemical Molecular Motion Using Noncovalent Interactions on Graphene and Its Application to Tailoring the Adsorption Energetics

Sayan Banerjee and Andrew M. Rappe*

Cite This: ACS Materials Lett. 2023, 5, 574–579

Read Online

ACCESS | Metrics & More | Article Recommendations | Supporting Information

ABSTRACT: **Herein we propose a new way to drive and control directional molecular motion on graphene by modifying the noncovalent interactions (NCIs). We show that molecules noncovalently interacting with graphene selectively diffuse away from the mountain (negative curvature) regions to the valley (positive curvature) regions. This is in contrast to previously reported molecular migration from the valley to the mountain of covalently attached molecules on graphene. To generalize the concept, we investigate a series of NCIs, including $\pi-\pi$, C−H−−π, lone pair−π, halogen−π, cation−π, and anion−π, and find the same robust trend. We further demonstrate that such directional motion of noncovalently bonded molecules can be exploited to create binding sites with tunable chemisorption energy on curved graphene. As a proof-of-concept demonstration, we consider the motion of strong electron acceptor tetracyanoquinodimethane (TCNQ) and show that a noticeable change in chemisorption energy can be attained for a set of adsorbates as a consequence of NCI-driven molecular migration of TCNQ. Thus, we propose that NCI-driven molecular migration can provide an additional controllable dimension to overcome the fundamental limitations of heterogeneous catalysis using 2D materials.**

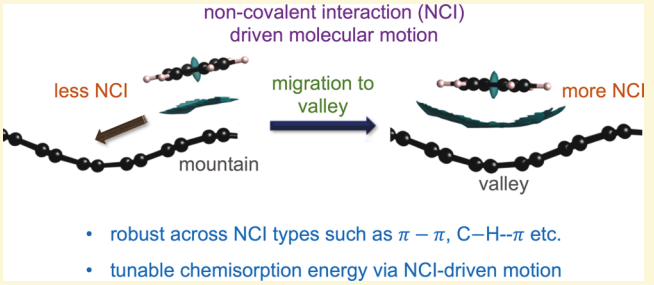

Research in the field of two-dimensional (2D) materials has skyrocketed in the last few decades because of their interesting light-matter interaction behavior,[1−6] applications in ferroelectrics,[7,8] piezoelectrics,[9,10] and catalysis,[11−16] and other fundamentally interesting condensed matter physics applications.[5,17−22] Atomically precise synthetic protocols and spectroscopic characterization tools have further fueled the growth, as they have enabled the design and realization of a broad range of 2D materials.[1,23−29] To this end, graphene specifically has garnered immense interest, due to its interesting electronic structure and consequent application in optoelectronics and catalysis.[17−19,30−32] In this regard, covalent functionalization and mechanical perturbations using strain have been established as one of the key methods to further tune its electronic structure.[33−49] The covalent chemistry of molecule-graphene interfaces can have a great potential impact in optoelectronics and catalysis.[40−48] Additionally, mechanochemical effects can help tune the reactivity of graphene, and this has been realized experimentally.[50−57] The reactivity modulation of graphene is proposed to happen due to a decrease in electron delocalization as an effect of applied strain and/or curvature.[51,55,56,58−61]

On the other hand, controlled molecular motion at the nanoscale provides a dynamic way to control material properties.[62−73] To this end, we have recently shown that mechanochemical (curvature-driven) directional molecular motion can be realized on graphene.[74] In that study, covalently functionalized graphene was considered to demonstrate the molecular migration of one C−C bond, and it was predicted that the molecules selectively migrate from the valley to the mountain regions of sinusoidally curved graphene. Such a process can also be exploited to dynamically tune the local defect states of graphene. Understanding and control of the

Received: October 27, 2022
Accepted: January 6, 2023
Published: January 18, 2023

https://doi.org/10.1021/acsmaterialslett.2c01021
ACS Materials Lett. 2023, 5, 574−579

defect states and their dynamics are crucial, because of their importance to physical and chemical response properties.[75−79]

Covalent functionalization generally perturbs the geometric structure of a material to alter its electronic structure and properties. On the other hand, a noncovalent interaction (NCI) can affect the electronic structure without inducing any strong geometric perturbation to a system and therefore can exert an additive effect. The NCI has been established as an extremely important component in different areas, including catalysis,[80,81] layered nanomaterials, materials growth and stability,[82,83] and solvation dynamics.[83,84] Although establishing the exact type of NCIs is often challenging due to their inherently nonlocal nature, different types of NCIs have been proposed. This includes $\pi-\pi$, C−H−π, lone pair-π, and halogen-π NCIs. In this regard, there exist multiple ways to combine mechanochemical perturbations of 2D materials and different types of NCIs, inspiring the design of multicomponent systems in order to perform molecular motion driven by NCIs. In such a system, mechanochemical effects can induce varying extents of NCIs in different spatial regions and therefore can provide a dynamic way to induce molecular motion and thereby to control the electronic structure of a 2D material without covalent functionalization.

The activity and selectivity of heterogeneous reactions are limited by the Sabatier volcano and scaling relations associated with the surface−adsorbate combinations.[85,86] To this end, Sabatier's principle considers the adsorption and desorption of an adsorbate and concludes that catalytic activity of a surface is limited by an optimum adsorbate binding strength and therefore follows a volcano shaped curve.[85] On the other hand, scaling relations indicate that the multidimensional nature of the catalytic activity can be portrayed with a linear model using one descriptor.[85,87] The nature of the descriptor varies from reaction to reaction; for example, the activity of N_2 to NH_3 conversion can be explained using the −N binding energy.[85] In this area, designing multicomponent systems is proposed as one of the ways to circumvent the fundamental limitations of heterogeneous catalysis.[88−91] As the molecular motion introduces a dynamic effect on the electronic structure of 2D materials, this NCI effect can potentially be harnessed to create binding sites with tunable adsorption energy.

In this study, we explore the effect of different NCIs on directional molecular diffusion on a curved graphene via density functional theory calculations. We investigate molecule-graphene interfaces having different types of NCIs, including $\pi-\pi$, C−H−π, lone pair−π, halogen−π, cation−π, and anion−π. We find that irrespective of the nature of the NCI, the molecules physisorb more strongly near the valley regions (positive curvature) rather than the mountain regions (negative curvature). This suggests that the molecules will move toward the valley regions, which is in contrast with the migration of covalently bonded molecules on graphene,[74] which prefer to go from the valley to the mountain. We then demonstrate that by judicious choice of the molecule and by capitalizing on its migration toward the valley sites, binding sites with tunable adsorption energy can be created on graphene. We conclude that NCI-driven molecular migration can provide an additional dimension in overcoming the limitations of heterogeneous catalysis.

The Effect of Noncovalent Interaction on Molecular Migration. We consider a sinusoidally curved graphene, which has valley (positive curvature) and mountain (negative curvature) sites, and such one-dimensional curvature can be attained experimentally.[33−39] In a previous work, we showed that one can attain directional molecular migration of a covalently attached aromatic adsorbate from the valley regions to the mountain regions.[74] Directional migration can happen, as the adsorbate has higher binding energy at the mountain site, which is a consequence of the concave-down/pyramidal geometry of the mountain regions. As the mountain sites have concave-down geometry, pyramidalization, which is the conversion from sp^2 to sp^3 hybridization upon functionalization, requires less energy at the mountain sites than the valley sites (concave up geometry). In other words, the mountain sites on unfunctionalized curved graphene provide greater disruption of the in-plane delocalization, giving them a closer resemblance to sp^3 pyramid-like centers. This causes a directional migration from the valley to the mountain for covalently bonded molecules because of this thermodynamic drive. On the other hand, this also suggests that because of the broken in-plane π-conjugation at the mountain sites, it should have a less prominent noncovalent interaction (NCI) with an adsorbate than the valley sites. This hypothesis stems from the fact that less conjugated (more localized) electrons near the mountain lead to lower polarizability and hence a lower extent of the NCI. This motivates us to explore the effect of the NCI on the molecular migration. The density functional theory (DFT) calculation details are provided in the Supporting Information.

To understand the effect of the NCI on molecular migration, we first explore the $\pi-\pi$ type of the NCI by taking benzene (C_6H_6) as a representative adsorbate (Figure 1a). We find that

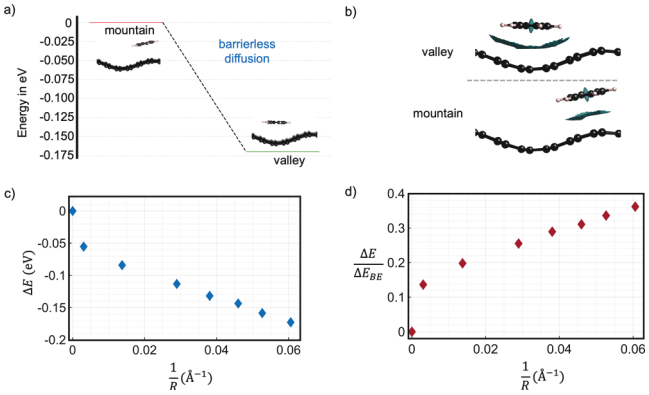

Figure 1. The influence of the $\pi-\pi$ noncovalent interaction on molecular migration: a) Migration of benzene on curved graphene. b) Noncovalent interaction (NCI) plot showing the interaction between the graphene and benzene. c) The relative stabilization ($E_{valley} - E_{mountain} = \Delta E$) as a function of the radius of curvature (R). d) The ratio between the relative stabilization at the valley site (ΔE) to the physisorption energy at the valley site (ΔE_{BE}).

the benzene noncovalently interacting with graphene is thermodynamically more stabilized near the valley than the mountain, which is in contrast to the covalent functionalization trend. This is comprehensible, as the concave-down (mountain) geometry is closer to sp^3, so therefore, the extent of NCI stabilization due to $\pi-\pi$ interaction is greater at the valley sites. This indicates that the benzene will diffuse away from the mountain sites and will concentrate near the valley sites because of the energy gain. We find that such migration from the mountain to the valley site is barrierless (Figure 1a), and hence, kinetically the molecule can rapidly move toward the

https://doi.org/10.1021/acsmaterialslett.2c01021
ACS Materials Lett. 2023, 5, 574−579

valley. In other words, the barrier of migration from one valley site to another one via a mountain site is 0.17 eV. To confirm the higher extent of NCIs at the valley sites than the mountain sites, we generate NCI plots (Figure 1b) wherein the reduced electron density gradient ($s = \frac{1}{2(3\pi^2)^{1/3}}\frac{|\nabla\rho|}{\rho^{4/3}}$) can capture the extent of the NCI.[92] Such a plot considers the electron density and reduced density gradient and captures the interactions in the low electron density regime.[92] The green shaded region between the graphene and the benzene indicates the extent of NCIs at the interface, and it portrays graphically the greater extent of NCIs at the valley (top panel in Figure 1b) than at the mountain (bottom panel in Figure 1b). Therefore, the results suggest that an adsorbate interacting noncovalently with graphene via $\pi-\pi$ stacking can undergo directional migration from the mountain to the valley sites. To understand the spatial scale to observe such migration, we calculate the stabilization at the valley site (ΔE) relative to the mountain site, as a function of the radius of curvature (R) (Figure 1c). We find that although ΔE decreases with increasing R, there is substantial thermodynamic drive to migrate toward the valley sites. To quantify the extent of the thermodynamic drive, we plot the ratio between the relative stabilization at the valley site (ΔE) and the physisorption energy (ΔE_{BE}) of benzene at the valley site, as a function of R (Figure 1d). We find that the ΔE_{BE} of benzene at the valley site is in the range of −0.41 to −0.48 eV. Therefore, a $\left(\frac{\Delta E}{\Delta E_{BE}}\right)$ value of 0.25 in Figure 1d corresponds to ≈0.10 eV of thermodynamic drive when the ΔE_{BE} is ≈−0.40 eV. Hence, we conclude that the thermodynamic drive is substantial enough to observe the $\pi-\pi$ NCI-driven migration for experimentally realizable curvatures and length scales.[93−97]

Next, we study a set of molecules representing different types of NCIs to see how migration depends on the type of the NCI (Figure 2a). We consider H_2O for $lp-\pi$, C_2H_6 for C−H−π, C_2F_6 for C−F−π, C_2H_4 for aliphatic $\pi-\pi$, Li for cation−π, and I for anion−π NCI (Figure 2a). We find that irrespective of the NCI type, the molecules prefer to stay near the valley site. This trend is shown clearly in Figure 2b, where (ΔE) represents the stabilization at the valley sites relative to the mountain sites. The different extent of stabilization is comprehensible, as these interactions correspond to different types of NCIs.[98,99] It is worth noting that the stabilization becomes more prominent as the conjugation in the aromatic ring increases (Figure 2b), i.e., naphthalene experiences more stabilization at the valley than benzene, and anthracene experiences more stabilization at the valley than naphthalene.

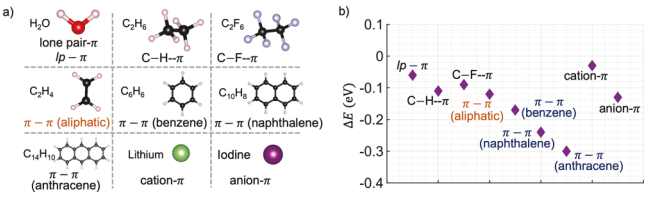

Figure 2. Comparison of various noncovalent interaction types and their influence on molecular migration: a) Details of the molecular systems considered to study the different types of NCIs. b) Effect of NCIs on the thermodynamic stability of the molecules at the mountain and valley sites. The relative stabilization at the valley site is ΔE.

Thus, we conclude that by tuning the nature of the aromatic adsorbate, one can tailor the thermodynamic drive and thereby further extend the spatial length-scale over which one can experimentally observe the migration process (Figure 1d). We also emphasize that the molecular migration from the mountain to the valley can be attained for a wide range of adsorbates, irrespective of the type of the NCI. As one can select the nature of the adsorbates, incorporating a range of chemical functionalities such as aromatic conjugation, electron-donating and/or electron-accepting groups, the directional migration provides a new dimension to tune the electronic structure of graphene in different regions without necessitating any covalent functionalization. To this end, we hypothesize that the NCI-driven migration can also create different binding sites on graphene, as the sites near the valley will have a different electronic and steric environment than the mountain sites.

Tuning Adsorption Energy Using NCI-Driven Molecular Migration. In this section, we investigate the possibility of tuning the energy of important reaction intermediates via NCI-driven molecular migration. To this end, we consider the migration of a strong electron acceptor adsorbate, tetracyanoquinodimethane (TCNQ), to induce changes in the electronic environment. The ΔE of TCNQ is −0.36 eV, where it is more stable at the valley site. As the covalent functionalization preferentially happens at the mountain sites, NCI-driven migration of TCNQ to the valley can influence the binding energy at the mountain site opposite to it (Figure 3a).

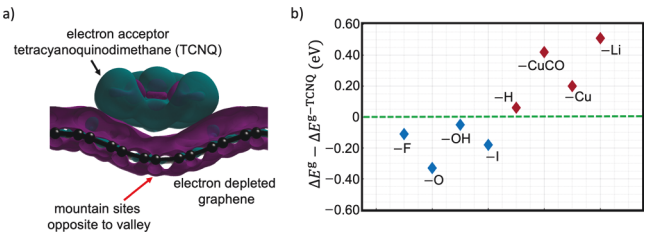

Figure 3. Tuning adsorption energy via molecular migration: a) Charge density difference plot showing the interaction between electron acceptor TCNQ and graphene and resulting electron transfer from the graphene to TCNQ. Magenta and teal colors correspond to electron depletion and accumulation, respectively. b) Difference in covalent binding energy of different adsorbates at mountain sites of curved graphene as a result of NCI-driven TCNQ migration to the valley sites on the opposite side. The binding energy of adsorbates in the absence of TCNQ is denoted as ΔE^g, and in the presence of TCNQ, it is denoted as ΔE^{g-TCNQ}.

Specifically, for monolayer graphene, the same in-plane location on the opposite of the valley is a mountain site; once the TCNQ molecule migrates to the valley site, the mountain site opposite should have a different electronic environment than the mountain sites with no TCNQ adsorbed underneath. As shown in the charge density difference plot (Figure 3a), we find that TCNQ creates electron depletion in the graphene through the NCI (charge transfer). To understand the effect of TCNQ migration on adsorption energy, we compare the (covalent) binding energy of adsorbates in the absence of TCNQ (ΔE^g) and in the presence of TCNQ (ΔE^{g-TCNQ}) on curved graphene. The binding energy of intermediates important for the hydrogen evolution reaction (HER), oxygen reduction reaction (ORR), and oxygen evolution reaction (OER), such as −H, −OH, and

https://doi.org/10.1021/acsmaterialslett.2c01021
ACS Materials Lett. 2023, 5, 574−579

−O, is considered. Furthermore, we consider intermediates which prefer different charge environments, such as −I, −F, −Cu, −CuCO, and −Li, as proof-of-concept examples to establish the binding energy tunability trend. We find that depending on the nature of the adsorbates, ΔE^{g-TCNQ} differs from ΔE^{g}. The green dashed line in Figure 3b corresponds to when there is no difference, a negative value in Figure 3b means a stronger binding at the graphene without TCNQ, and a positive value means stronger binding at the graphene with TCNQ on it. We find that the adsorbates which prefer an electron-rich environment, i.e., −F, −OH, −O, and −I, bind more weakly to graphene when TCNQ is present (Figure 3b). On the other hand, the adsorbates which prefer an electron-depleted environment, i.e., −Cu, −CuCO, and −Li, bind more strongly to graphene when TCNQ is present (Figure 2b). It is worth noting that adsorbates which have weak charge preference such as H have almost the same binding energy in both environments.

Therefore, we demonstrate that one can use molecular migration due to NCIs to create sites with tunable adsorption energies that can change the covalent binding energies of various functionalizing species. As adsorption and desorption energies are usually intrinsic to the adsorbing material and the adsorbate, catalytic processes are generally limited by a volcano-shaped curve, which is also referred to as the Sabatier principle in heterogeneous catalysis.[85−87,100] The peak of the volcano corresponds to the maximal activity, wherein the left or right side of the volcano represents too strong or too weak adsorption. One can envisage that rational choice of the molecule participating in the NCI-driven migration process can tailor both the adsorption and desorption energies. Therefore, the limitations imposed by the Sabatier principle can be potentially lifted. Thus, we propose that a multi-component system can be designed where molecular migration can dynamically control the adsorption and desorption processes, i.e., molecular motion assisted adsorption/desorption can happen at nearby spatial locations, and thus, it can break the scaling relations in catalytic processes.

Conclusions. Overall, we demonstrate that directional molecular motion from the mountain to the valley can be attained on graphene by leveraging the NCI. This is in contrast to the migration from valley to the mountain of a covalently attached molecule. Additionally, we showcase that this migration trend holds across various types of NCIs. Hence, the covalent and noncovalent interactions provide opposite molecular migration directions. In this regard, judicious choice of the interaction type and nature of the migrating molecule can help tailor the electronic structure of two-dimensional (2D) materials via a molecular additive effect. We furthermore demonstrate that such NCI-driven migration can help create binding sites with tunable chemisorption energy without introducing any geometric perturbation and therefore can improve the efficiency of catalytic reactions on graphene. The results indicate that molecular migration can be explored to design multicomponent 2D systems to transcend the limitations of heterogeneous catalytic reactions.

■ ASSOCIATED CONTENT

Supporting Information

The Supporting Information is available free of charge at https://pubs.acs.org/doi/10.1021/acsmaterialslett.2c01021.

Density functional theory calculation parameters; graphene supercell details (PDF)

■ AUTHOR INFORMATION

Corresponding Author

Andrew M. Rappe − *Department of Chemistry, University of Pennsylvania, Philadelphia, Pennsylvania 19104-6323, United States;* orcid.org/0000-0003-4620-6496; Email: rappe@sas.upenn.edu

Author

Sayan Banerjee − *Department of Chemistry, University of Pennsylvania, Philadelphia, Pennsylvania 19104-6323, United States;* orcid.org/0000-0002-8586-9236

Complete contact information is available at: https://pubs.acs.org/10.1021/acsmaterialslett.2c01021

Notes

The authors declare no competing financial interest.

■ ACKNOWLEDGMENTS

The work is supported by the NSF Center for the Mechanical Control of Chemistry under grant CHE-2023644. S.B. acknowledges the Vagelos Institute for Energy Science and Technology for the graduate fellowship. A.M.R. acknowledges support from the U.S. Department of Energy, Office of Science, Basic Energy Sciences, under Award # DE-SC0019281. Computational support was provided by the National Energy Research Scientific Computing Center (NERSC).

■ REFERENCES

(1) Bernardi, M.; Palummo, M.; Grossman, J. C. Extraordinary Sunlight Absorption and One Nanometer Thick Photovoltaics Using Two-Dimensional Monolayer Materials. *Nano Lett.* **2013**, *13*, 3664−3670.

(2) Berry, J.; et al. Hybrid Organic-Inorganic Perovskites (HOIPs): Opportunities and Challenges. *Adv. Mater.* **2015**, *27*, 5102−5112.

(3) Li, W.; Wang, Z.; Deschler, F.; Gao, S.; Friend, R. H.; Cheetham, A. K. Chemically diverse and multifunctional hybrid organic−inorganic perovskites. *Nature Reviews Materials* **2017**, *2*, 16099.

(4) Schankler, A. M.; Gao, L.; Rappe, A. M. Large Bulk Piezophotovoltaic Effect of Monolayer 2H-MoS_2. *J. Phys. Chem. Lett.* **2021**, *12*, 1244−1249.

(5) Bhimanapati, G. R.; et al. Recent Advances in Two-Dimensional Materials beyond Graphene. *ACS Nano* **2015**, *9*, 11509−11539.

(6) del Corro, E.; Terrones, H.; Elias, A.; Fantini, C.; Feng, S.; Nguyen, M. A.; Mallouk, T. E.; Terrones, M.; Pimenta, M. A. Excited Excitonic States in 1L, 2L, 3L, and Bulk WSe_2 Observed by Resonant Raman Spectroscopy. *ACS Nano* **2014**, *8*, 9629−9635.

(7) Martin, L. W.; Rappe, A. M. Thin-film ferroelectric materials and their applications. *Nature Reviews Materials* **2017**, *2*, 16087.

(8) Wu, M.; Jena, P. The rise of two-dimensional van der Waals ferroelectrics. *Wiley Interdisciplinary Reviews: Computational Molecular Science* **2018**, *8*, e1365.

(9) Qi, Y.; Rappe, A. M. Widespread negative longitudinal piezoelectric responses in ferroelectric crystals with layered structures. *Phys. Rev. Lett.* **2021**, *126*, 217601.

(10) Liu, S.; Cohen, R. Origin of negative longitudinal piezoelectric effect. *Phys. Rev. Lett.* **2017**, *119*, 207601.

(11) Voiry, D.; Shin, H. S.; Loh, K. P.; Chhowalla, M. Low-dimensional catalysts for hydrogen evolution and CO_2 reduction. *Nature Reviews Chemistry* **2018**, *2*, 0105.

(12) Seh, Z. W.; Fredrickson, K. D.; Anasori, B.; Kibsgaard, J.; Strickler, A. L.; Lukatskaya, M. R.; Gogotsi, Y.; Jaramillo, T. F.;

Vojvodic, A. Two-Dimensional Molybdenum Carbide (MXene) as an Efficient Electrocatalyst for Hydrogen Evolution. *ACS Energy Letters* **2016**, *1*, 589−594.
(13) Gusmão, R.; Veselý, M.; Sofer, Z. Recent Developments on the Single Atom Supported at 2D Materials Beyond Graphene as Catalysts. *ACS Catal.* **2020**, *10*, 9634−9648.
(14) Chia, X.; Pumera, M. Characteristics and performance of two-dimensional materials for electrocatalysis. *Nature Catalysis* **2018**, *1*, 909−921.
(15) Siahrostami, S.; Tsai, C.; Karamad, M.; Koitz, R.; García-Melchor, M.; Bajdich, M.; Vojvodic, A.; Abild-Pedersen, F.; Nørskov, J. K.; Studt, F. Two-Dimensional Materials as Catalysts for Energy Conversion. *Catal. Lett.* **2016**, *146*, 1917−1921.
(16) Bollinger, M.; Lauritsen, J.; Jacobsen, K. W.; Nørskov, J. K.; Helveg, S.; Besenbacher, F. One-dimensional metallic edge states in MoS_2. *Physical review letters* **2001**, *87*, 196803.
(17) Young, S. M.; Kane, C. L. Dirac semimetals in two dimensions. *Physical review letters* **2015**, *115*, 126803.
(18) Kane, C. L.; Mele, E. J. Z_2 topological order and the quantum spin Hall effect. *Physical review letters* **2005**, *95*, 146802.
(19) Kane, C. L.; Mele, E. J. Quantum spin Hall effect in graphene. *Physical review letters* **2005**, *95*, 226801.
(20) Schaibley, J. R.; Yu, H.; Clark, G.; Rivera, P.; Ross, J. S.; Seyler, K. L.; Yao, W.; Xu, X. Valleytronics in 2D materials. *Nature Reviews Materials* **2016**, *1*, 16055.
(21) Tartakovskii, A. Excitons in 2D heterostructures. *Nature Reviews Physics* **2020**, *2*, 8−9.
(22) Wilson, N. P.; Yao, W.; Shan, J.; Xu, X. Excitons and emergent quantum phenomena in stacked 2D semiconductors. *Nature* **2021**, *599*, 383−392.
(23) Dong, R.; Zhang, T.; Feng, X. Interface-Assisted Synthesis of 2D Materials: Trend and Challenges. *Chem. Rev.* **2018**, *118*, 6189−6235.
(24) Huang, L.; Hu, Z.; Jin, H.; Wu, J.; Liu, K.; Xu, Z.; Wan, J.; Zhou, H.; Duan, J.; Hu, B.; Zhou, J. Salt-Assisted Synthesis of 2D Materials. *Adv. Funct. Mater.* **2020**, *30*, 1908486.
(25) Zhou, J.; et al. A library of atomically thin metal chalcogenides. *Nature* **2018**, *556*, 355−359.
(26) Novoselov, K. S.; Geim, A. K.; Morozov, S. V.; Jiang, D.; Zhang, Y.; Dubonos, S. V.; Grigorieva, I. V.; Firsov, A. A. Electric Field Effect in Atomically Thin Carbon Films. *Science* **2004**, *306*, 666−669.
(27) Lin, Z.; et al. 2D materials advances: from large scale synthesis and controlled heterostructures to improved characterization techniques, defects and applications. *2D Materials* **2016**, *3*, 042001.
(28) Mas-Balleste, R.; Gómez-Navarro, C.; Gómez-Herrero, J.; Zamora, F. 2D materials: to graphene and beyond. *Nanoscale* **2011**, *3*, 20−30.
(29) Gupta, A.; Sakthivel, T.; Seal, S. Recent development in 2D materials beyond graphene. *Prog. Mater. Sci.* **2015**, *73*, 44−126.
(30) Higgins, D.; Zamani, P.; Yu, A.; Chen, Z. The application of graphene and its composites in oxygen reduction electrocatalysis: a perspective and review of recent progress. *Energy Environ. Sci.* **2016**, *9*, 357−390.
(31) Huang, C.; Li, C.; Shi, G. Graphene based catalysts. *Energy Environ. Sci.* **2012**, *5*, 8848.
(32) Li, X.; Yu, J.; Wageh, S.; Al-Ghamdi, A. A.; Xie, J. Graphene in Photocatalysis: A Review. *Small* **2016**, *12*, 6640−6696.
(33) Gao, T.; Xie, S.; Gao, Y.; Liu, M.; Chen, Y.; Zhang, Y.; Liu, Z. Growth and Atomic-Scale Characterizations of Graphene on Multi-faceted Textured Pt Foils Prepared by Chemical Vapor Deposition. *ACS Nano* **2011**, *5*, 9194−9201.
(34) Zhang, Y.; Gao, T.; Gao, Y.; Xie, S.; Ji, Q.; Yan, K.; Peng, H.; Liu, Z. Defect-like Structures of Graphene on Copper Foils for Strain Relief Investigated by High−Resolution Scanning Tunneling Microscopy. *ACS Nano* **2011**, *5*, 4014−4022.
(35) Ishigami, M.; Chen, J. H.; Cullen, W. G.; Fuhrer, M. S.; Williams, E. D. Atomic Structure of Graphene on SiO_2. *Nano Lett.* **2007**, *7*, 1643−1648.
(36) Venema, L. C.; Meunier, V.; Lambin, P.; Dekker, C. Atomic structure of carbon nanotubes from scanning tunneling microscopy. *Phys. Rev. B* **2000**, *61*, 2991−2996.
(37) Yan, W.; He, W.-Y.; Chu, Z.-D.; Liu, M.; Meng, L.; Dou, R.-F.; Zhang, Y.; Liu, Z.; Nie, J.-C.; He, L. Strain and curvature induced evolution of electronic band structures in twisted graphene bilayer. *Nat. Commun.* **2013**, *4*, 2159.
(38) Meyer, J. C.; Geim, A. K.; Katsnelson, M. I.; Novoselov, K. S.; Booth, T. J.; Roth, S. The structure of suspended graphene sheets. *Nature* **2007**, *446*, 60−63.
(39) Thompson-Flagg, R. C.; Moura, M. J. B.; Marder, M. Rippling of graphene. *EPL (Europhysics Letters)* **2009**, *85*, 46002.
(40) Jackson, M. N.; Kaminsky, C. J.; Oh, S.; Melville, J. F.; Surendranath, Y. Graphite Conjugation Eliminates Redox Intermediates in Molecular Electrocatalysis. *J. Am. Chem. Soc.* **2019**, *141*, 14160−14167.
(41) Jackson, M. N.; Oh, S.; Kaminsky, C. J.; Chu, S. B.; Zhang, G.; Miller, J. T.; Surendranath, Y. Strong Electronic Coupling of Molecular Sites to Graphitic Electrodes via Pyrazine Conjugation. *J. Am. Chem. Soc.* **2018**, *140*, 1004−1010.
(42) Schultz, B. J.; Dennis, R. V.; Lee, V.; Banerjee, S. An electronic structure perspective of graphene interfaces. *Nanoscale* **2014**, *6*, 3444−3466.
(43) Liu, L.-M.; Car, R.; Selloni, A.; Dabbs, D. M.; Aksay, I. A.; Yetter, R. A. Enhanced Thermal Decomposition of Nitromethane on Functionalized Graphene Sheets: Ab Initio Molecular Dynamics Simulations. *J. Am. Chem. Soc.* **2012**, *134*, 19011−19016.
(44) Zhang, C.; Dabbs, D. M.; Liu, L.-M.; Aksay, I. A.; Car, R.; Selloni, A. Combined Effects of Functional Groups, Lattice Defects, and Edges in the Infrared Spectra of Graphene Oxide. *J. Phys. Chem. C* **2015**, *119*, 18167−18176.
(45) Ping, J.; Vishnubhotla, R.; Vrudhula, A.; Johnson, A. T. C. Scalable Production of High-Sensitivity, Label-Free DNA Biosensors Based on Back-Gated Graphene Field Effect Transistors. *ACS Nano* **2016**, *10*, 8700−8704.
(46) Kumar, N.; Wang, W.; Ortiz-Marquez, J. C.; Catalano, M.; Gray, M.; Biglari, N.; Hikari, K.; Ling, X.; Gao, J.; van Opijnen, T.; Burch, K. S. Dielectrophoresis assisted rapid, selective and single cell detection of antibiotic resistant bacteria with G-FETs. *Biosens. Bioelectron.* **2020**, *156*, 112123.
(47) Park, I.; Lim, J.; You, S.; Hwang, M. T.; Kwon, J.; Koprowski, K.; Kim, S.; Heredia, J.; Stewart de Ramirez, S. A.; Valera, E.; Bashir, R. Detection of SARS-CoV-2 Virus Amplification Using a Crumpled Graphene Field-Effect Transistor Biosensor. *ACS Sensors* **2021**, *6*, 4461−4470.
(48) Liou, F.; Tsai, H.-Z.; Aikawa, A. S.; Natividad, K. C.; Tang, E.; Ha, E.; Riss, A.; Watanabe, K.; Taniguchi, T.; Lischner, J.; Zettl, A.; Crommie, M. F. Imaging Reconfigurable Molecular Concentration on a Graphene Field-Effect Transistor. *Nano Lett.* **2021**, *21*, 8770−8776.
(49) He, M.; Swager, T. M. Aryl Migration on Graphene. *J. Am. Chem. Soc.* **2020**, *142*, 17876−17880.
(50) Wu, Q.; Wu, Y.; Hao, Y.; Geng, J.; Charlton, M.; Chen, S.; Ren, Y.; Ji, H.; Li, H.; Boukhvalov, D. W.; Piner, R. D.; Bielawski, C. W.; Ruoff, R. S. Selective surface functionalization at regions of high local curvature in graphene. *Chem. Commun.* **2013**, *49*, 677−679.
(51) Boukhvalov, D. W.; Katsnelson, M. I. Enhancement of Chemical Activity in Corrugated Graphene. *J. Phys. Chem. C* **2009**, *113*, 14176−14178.
(52) Deng, S.; Rhee, D.; Lee, W.-K.; Che, S.; Keisham, B.; Berry, V.; Odom, T. W. Graphene Wrinkles Enable Spatially Defined Chemistry. *Nano Lett.* **2019**, *19*, 5640−5646.
(53) Bissett, M. A.; Konabe, S.; Okada, S.; Tsuji, M.; Ago, H. Enhanced Chemical Reactivity of Graphene Induced by Mechanical Strain. *ACS Nano* **2013**, *7*, 10335−10343.
(54) Nguyen, M.-T. An ab initio study of oxygen on strained graphene. *J. Phys.: Condens. Matter* **2013**, *25*, 395301.
(55) Qu, Y.; Ke, Y.; Shao, Y.; Chen, W.; Kwok, C. T.; Shi, X.; Pan, H. Effect of Curvature on the Hydrogen Evolution Reaction of Graphene. *J. Phys. Chem. C* **2018**, *122*, 25331−25338.

(56) Shen, Y.; Dai, E.; Liu, X.; Pan, W.; Yang, H.; Xiong, B.; Zerulla, D. Curvature analysis of single layer graphene on the basis of extreme low-frequency Raman spectroscopy. *Appl. Phys. Lett.* **2019**, *114*, 161907.
(57) Wang, G.; Dai, Z.; Xiao, J.; Feng, S.; Weng, C.; Liu, L.; Xu, Z.; Huang, R.; Zhang, Z. Bending of multilayer van der Waals materials. *Phys. Rev. Lett.* **2019**, *123*, 116101.
(58) Haddon, R. C. Chemistry of the Fullerenes: The Manifestation of Strain in a Class of Continuous Aromatic Molecules. *Science* **1993**, *261*, 1545−1550.
(59) Haddon, R. C. Hybridization and the orientation and alignment of π-orbitals in nonplanar conjugated organic molecules: π-orbital axis vector analysis (POAV2). *J. Am. Chem. Soc.* **1986**, *108*, 2837−2842.
(60) Haddon, R. C. Rehybridization and π-orbital overlap in nonplanar conjugated organic molecules: π-orbital axis vector (POAV) analysis and three-dimensional Hueckel molecular orbital (3D-HMO) theory. *J. Am. Chem. Soc.* **1987**, *109*, 1676−1685.
(61) Haddon, R. C. Pyramidalization: geometrical interpretation of the π-orbital axis vector in three dimensions. *J. Phys. Chem.* **1987**, *91*, 3719−3720.
(62) van den Heuvel, M. G. L.; Dekker, C. Motor Proteins at Work for Nanotechnology. *Science* **2007**, *317*, 333−336.
(63) Schliwa, M.; Woehlke, G. Molecular motors. *Nature* **2003**, *422*, 759−765.
(64) Anelli, P. L.; Spencer, N.; Stoddart, J. F. A molecular shuttle. *J. Am. Chem. Soc.* **1991**, *113*, 5131−5133.
(65) Bissell, R. A.; Córdova, E.; Kaifer, A. E.; Stoddart, J. F. A chemically and electrochemically switchable molecular shuttle. *Nature* **1994**, *369*, 133−137.
(66) Browne, W. R.; Feringa, B. L. Making molecular machines work. *Nat. Nanotechnol.* **2006**, *1*, 25−35.
(67) von Delius, M. v.; Leigh, D. A. Walking molecules. *Chem. Soc. Rev.* **2011**, *40*, 3656−3676.
(68) Feynman, R.*Feynman and computation*; CRC Press: 2018; pp 63−76, DOI: 10.1201/9780429500459-7.
(69) Koumura, N.; Zijlstra, R. W. J.; van Delden, R. A.; Harada, N.; Feringa, B. L. Light-driven monodirectional molecular rotor. *Nature* **1999**, *401*, 152−155.
(70) Kudernac, T.; Ruangsupapichat, N.; Parschau, M.; Maciá, B.; Katsonis, N.; Harutyunyan, S. R.; Ernst, K.-H.; Feringa, B. L. Electrically driven directional motion of a four-wheeled molecule on a metal surface. *Nature* **2011**, *479*, 208−211.
(71) Livoreil, A.; Dietrich-Buchecker, C. O.; Sauvage, J.-P. Electrochemically Triggered Swinging of a [2]-Catenate. *J. Am. Chem. Soc.* **1994**, *116*, 9399−9400.
(72) Vives, G.; Tour, J. M. Synthesis of Single-Molecule Nanocars. *Acc. Chem. Res.* **2009**, *42*, 473−487.
(73) von Delius, M.; Geertsema, E. M.; Leigh, D. A. A synthetic small molecule that can walk down a track. *Nat. Chem.* **2010**, *2*, 96−101.
(74) Banerjee, S.; Rappe, A. M. Mechanochemical Molecular Migration on Graphene. *J. Am. Chem. Soc.* **2022**, *144*, 7181−7188.
(75) Zou, X.; Yakobson, B. I. An Open Canvas— 2D Materials with Defects, Disorder, and Functionality. *Acc. Chem. Res.* **2015**, *48*, 73−80.
(76) Egger, D. A.; Bera, A.; Cahen, D.; Hodes, G.; Kirchartz, T.; Kronik, L.; Lovrincic, R.; Rappe, A. M.; Reichman, D. R.; Yaffe, O. What Remains Unexplained about the Properties of Halide Perovskites? *Adv. Mater.* **2018**, *30*, 1800691.
(77) Cohen, A. V.; Egger, D. A.; Rappe, A. M.; Kronik, L. Breakdown of the Static Picture of Defect Energetics in Halide Perovskites: The Case of the Br Vacancy in CsPbBrsub3/sub. *J. Phys. Chem. Lett.* **2019**, *10*, 4490−4498.
(78) Wexler, R. B.; Gautam, G. S.; Stechel, E. B.; Carter, E. A. Factors Governing Oxygen Vacancy Formation in Oxide Perovskites. *J. Am. Chem. Soc.* **2021**, *143*, 13212−13227.
(79) Kim, Y.-H.; Kim, S.; Kakekhani, A.; Park, J.; Park, J.; Lee, Y.-H.; Xu, H.; Nagane, S.; Wexler, R. B.; Kim, D.-H.; et al. Comprehensive defect suppression in perovskite nanocrystals for high-efficiency light-emitting diodes. *Nat. Photonics* **2021**, *15*, 148−155.
(80) Neel, A. J.; Hilton, M. J.; Sigman, M. S.; Toste, F. D. Exploiting non-covalent interactions for catalyst design. *Nature* **2017**, *543*, 637−646.
(81) Sunoj, R. B. Transition State Models for Understanding the Origin of Chiral Induction in Asymmetric Catalysis. *Acc. Chem. Res.* **2016**, *49*, 1019−1028.
(82) Geim, A. K.; Grigorieva, I. V. Van der Waals heterostructures. *Nature* **2013**, *499*, 419−425.
(83) Mahadevi, A. S.; Sastry, G. N. Cooperativity in Noncovalent Interactions. *Chem. Rev.* **2016**, *116*, 2775−2825.
(84) Müller-Dethlefs, K.; Hobza, P. Noncovalent Interactions: A Challenge for Experiment and Theory. *Chem. Rev.* **2000**, *100*, 143−168.
(85) Nørskov, J. K.; Studt, F.; Abild-Pedersen, F.; Bligaard, T.*Fundamental concepts in heterogeneous catalysis*; John Wiley & Sons: 2014; DOI: 10.1002/9781118892114.
(86) Nørskov, J. K.; Abild-Pedersen, F.; Studt, F.; Bligaard, T. Density functional theory in surface chemistry and catalysis. *Proc. Natl. Acad. Sci. U. S. A.* **2011**, *108*, 937−943.
(87) Nørskov, J. K.; Rossmeisl, J.; Logadottir, A.; Lindqvist, L.; Kitchin, J. R.; Bligaard, T.; Jónsson, H. Origin of the Overpotential for Oxygen Reduction at a Fuel-Cell Cathode. *J. Phys. Chem. B* **2004**, *108*, 17886−17892.
(88) Cao, A.; Bukas, V. J.; Shadravan, V.; Wang, Z.; Li, H.; Kibsgaard, J.; Chorkendorff, I.; Nørskov, J. K. A spin promotion effect in catalytic ammonia synthesis. *Nat. Commun.* **2022**, *13*, 2382.
(89) Kakekhani, A.; Ismail-Beigi, S.; Altman, E. I. Ferroelectrics: A pathway to switchable surface chemistry and catalysis. *Surf. Sci.* **2016**, *650*, 302−316.
(90) Qiu, T.; Tu, B.; Saldana-Greco, D.; Rappe, A. M. Ab Initio Simulation Explains the Enhancement of Catalytic Oxygen Evolution on $CaMnO_3$. *ACS Catal.* **2018**, *8*, 2218−2224.
(91) Ardagh, M. A.; Abdelrahman, O. A.; Dauenhauer, P. J. Principles of Dynamic Heterogeneous Catalysis: Surface Resonance and Turnover Frequency Response. *ACS Catal.* **2019**, *9*, 6929−6937.
(92) Contreras-García, J.; Johnson, E. R.; Keinan, S.; Chaudret, R.; Piquemal, J.-P.; Beratan, D. N.; Yang, W. NCIPLOT: A Program for Plotting Noncovalent Interaction Regions. *J. Chem. Theory Comput.* **2011**, *7*, 625−632.
(93) Hawthorne, N.; Banerjee, S.; Moore, Q.; Rappe, A. M.; Batteas, J. D. Studies of the Reactivity of Graphene Driven by Mechanical Distortions. *J. Phys. Chem. C* **2022**, *126*, 17569−17578.
(94) Falvo, M. R.; Clary, G.; Taylor, R. n.; Chi, V.; Brooks, F.; Washburn, S.; Superfine, R. Bending and buckling of carbon nanotubes under large strain. *Nature* **1997**, *389*, 582−584.
(95) Cheung, C. L.; Hafner, J. H.; Lieber, C. M. Carbon nanotube atomic force microscopy tips: Direct growth by chemical vapor deposition and application to high-resolution imaging. *Proc. Natl. Acad. Sci. U. S. A.* **2000**, *97*, 3809−3813.
(96) Imadate, K.; Hirahara, K. Experimental determination of the diameter-dependent wettability of carbon nanotubes as studied using atomic force microscopy. *Phys. Chem. Chem. Phys.* **2018**, *20*, 26979−26985.
(97) Gotovac, S.; Honda, H.; Hattori, Y.; Takahashi, K.; Kanoh, H.; Kaneko, K. Effect of Nanoscale Curvature of Single-Walled Carbon Nanotubes on Adsorption of Polycyclic Aromatic Hydrocarbons. *Nano Lett.* **2007**, *7*, 583−587.
(98) Britz, D. A.; Khlobystov, A. N. Noncovalent interactions of molecules with single walled carbon nanotubes. *Chem. Soc. Rev.* **2006**, *35*, 637.
(99) Hohenstein, E. G.; Sherrill, C. D. Wavefunction methods for noncovalent interactions. *Wiley Interdisciplinary Reviews: Computational Molecular Science* **2012**, *2*, 304−326.
(100) Kakekhani, A.; Roling, L. T.; Kulkarni, A.; Latimer, A. A.; Abroshan, H.; Schumann, J.; AlJama, H.; Siahrostami, S.; Ismail-Beigi, S.; Abild-Pedersen, F.; et al. Nature of lone-pair-surface bonds and their scaling relations. *Inorg. Chem.* **2018**, *57*, 7222−7238.